

# Occurrence of Uncommon Infinite Chains Consisting of Edge-Sharing Octahedra in a Porous Metal Organic Framework-Type Aluminum Pyromellitate $\text{Al}_4(\text{OH})_8[\text{C}_{10}\text{O}_8\text{H}_2]$ (MIL-120): Synthesis, Structure, and Gas Sorption Properties

Christophe Volkringer,<sup>†</sup> Thierry Loiseau,<sup>\*,†</sup> Mohamed Haouas,<sup>‡</sup> Francis Taulelle,<sup>‡</sup> Dmitry Popov,<sup>§</sup> Manfred Burghammer,<sup>§</sup> Christian Riekkel,<sup>§</sup> Claudia Zlotea,<sup>||</sup> Fermin Cuevas,<sup>||</sup> Michel Latroche,<sup>||</sup> Delphine Phanon,<sup>⊥</sup> Christina Knöfel,<sup>⊥</sup> Philip L Llewellyn,<sup>⊥</sup> and Gérard Férey<sup>†</sup>

<sup>†</sup>Porous Solids Group and <sup>‡</sup>Tectospin Group, Institut Lavoisier de Versailles (UMR CNRS 8180), Institut Universitaire de France, Université de Versailles Saint Quentin en Yvelines, 45, avenue des États-Unis, 78035 Versailles, France, <sup>§</sup>ESRF, 6, rue Jules Horowitz, B.P. 220, 38043 Grenoble cedex, France, <sup>||</sup>ICMPE-CMTR (UMR CNRS 7182), 2-8 rue Henri Dunant, 94320 Thiais, France, and <sup>⊥</sup>Laboratoire Chimie Provence (UMR CNRS 6264), Universités Aix-Marseille I, II, III, Centre de St Jérôme, 13013 Marseille cedex 20, France

Received July 28, 2009. Revised Manuscript Received October 9, 2009

A new metal organic framework (MOF)-type aluminum pyromellitate or  $\text{Al}_4(\text{OH})_8[\text{C}_{10}\text{O}_8\text{H}_2] \cdot 4.8-5\text{H}_2\text{O}$  (called MIL-120) has been hydrothermally synthesized at 210 °C for 24 h. Its structure was analyzed by single-crystal microdiffraction using the synchrotron radiation beamline at ID13 station (ESRF, Grenoble). It consists of infinite chains of aluminum centers in octahedral coordination connected to each other through the pyromellitate linker. The structural feature is the existence of the  $\text{AlO}_2(\text{OH})_4$  octahedra linked to each other via a common edge consisting of two  $\mu_2$ -hydroxo groups, along the [102] direction. The different positions of the common edge in the two distinct Al crystallographical sites induce a cis–trans connection mode of the octahedral units, and zigzag chains are generated. All the carboxylate groups of the pyromellitate molecules are perpendicularly connected to the inorganic chains, and it results in the formation of channels running along the *c* axis ( $5.4 \times 4.7$  Å), in which water molecules are encapsulated. <sup>27</sup>Al solid state NMR revealed two well resolved signals with two distinct quadrupolar coupling constants ( $C_Q = 8.07$  and  $4.77$  MHz) related to two Al sites. Brunnauer-Emmett-Teller (BET) surface area is  $308(4) \text{ m}^2 \text{ g}^{-1}$  (Langmuir:  $432(1) \text{ m}^2 \text{ g}^{-1}$ ).  $\text{H}_2$  adsorption is 1.3 wt % at 77 K and 3 MPa.  $\text{CH}_4$  or  $\text{CO}_2$  adsorptions are  $1.8 \text{ mmol g}^{-1}$  and  $4.8 \text{ mmol g}^{-1}$ , respectively, at 303 K (under 1 MPa).

## Introduction

For the past decade, intensive studies have been focused on the elaboration of porous hybrid materials involving metallic centers associated to organic ligands. Such compounds, commonly named metal organic framework (MOF) or coordination polymers, exhibit crystalline organized pore systems with well-defined size and geometry.<sup>1–3</sup> These materials are promising to many industrial applications in the fields of molecular storage, separation, catalysis, etc.<sup>4,5</sup> A large number of solids was already reported, involving different cations

(mostly divalent metals) with multidentate carboxylate linkers. Among them, the trivalent ion aluminum was found to be a good candidate for the generation of three-dimensional networks with noticeable porosity and low density. Different compounds have, thus, been isolated with the ligands terephthalate (MIL-53<sup>6</sup>), amino-terephthalate (CAU-1),<sup>7</sup> 2,6-naphthalenedicarboxylate (MIL-69,<sup>8</sup> DUT-4<sup>9</sup>), 1,4-naphthalenedicarboxylate,<sup>10</sup> 4,4'-biphenyldicarboxylate (DUT-5<sup>9</sup>), trimesate (MIL-96,<sup>11</sup>

\*To whom correspondence should be addressed. E-mail: thierry.loiseau@ensc-lille.fr. Phone: (33) 3 20 43 44 34. Fax: (33) 3 20 43 48 95. Present address: Unité de Catalyse et Chimie du Solide (UCCS)–UMR CNRS 8181–Université de Lille, 59652 Villeneuve d'Ascq, France.

(1) Férey, G. *Chem. Soc. Rev.* **2008**, *37*, 191.  
(2) Yaghi, O. M.; O'Keeffe, M.; Ockwig, N. W.; Chae, H. K.; Eddaoudi, M.; Kim, J. *Nature* **2003**, *423*, 705.  
(3) Kitagawa, S.; Kitaura, R.; Noro, S.-I. *Angew. Chem., Int. Ed.* **2004**, *43*, 2334.  
(4) Janiak, C. *Dalton Trans.* **2003**, 2781.  
(5) Czaja, A. U.; Trukhan, N.; Müller, U. *Chem. Soc. Rev.* **2009**, *38*, 1284.

(6) Loiseau, T.; Serre, C.; Huguenard, C.; Fink, G.; Taulelle, F.; Henry, M.; Bataille, T.; Férey, G. *Chem.—Eur. J.* **2004**, *10*, 1373.  
(7) Ahnfeldt, T.; Guillou, N.; Gunzelmann, D.; Margiolaki, I.; Loiseau, T.; Férey, G.; Senker, J.; Stock *Angew. Chem., Int. Ed.* **2009**, *48*, 5163.  
(8) Loiseau, T.; Mellot-Draznieks, C.; Muguerra, H.; Férey, G.; Haouas, M.; Taulelle, F. *C. R. Chimie* **2005**, *8*, 765.  
(9) Senkowska, I.; Hoffmann, F.; Fröba, M.; Getzschmann, J.; Böhlmann, W.; Kaskel, S. *Microporous Mesoporous Mater.* **2009**, *122*, 93.  
(10) Comotti, A.; Bracco, S.; Sozzani, O.; Horike, S.; Matsuda, R.; Chen, J.; Takata, M.; Kubota, Y.; Kitagawa, S. *J. Am. Chem. Soc.* **2008**, *130*, 13664.  
(11) Loiseau, T.; Lecroq, L.; Volkringer, C.; Marrot, J.; Férey, G.; Haouas, M.; Taulelle, F.; Bourrelly, S.; Llewellyn, P. L.; Latroche, M. *J. Am. Chem. Soc.* **2006**, *128*, 10223.

MIL-110<sup>12</sup>) 1,4,5,8-naphthalenetetracarboxylate (MIL-122<sup>13</sup>), or pyromellitate (MIL-118<sup>14</sup>). From the structural point of view, one of the common features (except MIL-110 and CAU-1) is the existence of the chains of octahedrally coordinated aluminum cations linked to each other via a  $\mu_2$ -hydroxo corner. In these structures, the three-dimensional cohesion is ensured by the carboxylate molecules, which connect the inorganic chains to each other.

During our investigations on the reactivity of the pyromellitate (1,2,4,5-benzenetetracarboxylate) with aluminum, we recently observed the hydrothermal crystallization of a new compound (MIL-118<sup>14</sup>), which is close to the MIL-53<sup>6</sup> archetype. The study of the phase diagram allowed us to isolate a second phase by varying the reaction pH adjusted with NaOH. Considering the organic part, the pyromellitate linker was previously employed with other trivalent elements such as vanadium,<sup>15</sup> gallium,<sup>16</sup> or indium.<sup>17–19</sup> It was observed to have the formation of a quite open network, in the case of indium ( $\text{In}_3(\text{C}_{10}\text{O}_8\text{H}_2)_2(\text{OH})_2$ <sup>18</sup>), with a potential accessible pore volume up to 43.3%. Here, this contribution deals with the synthesis and the structural characterization of the new aluminum pyromellitate, called MIL-120 (Materials Institut Lavoisier) or  $\text{Al}_4(\text{OH})_8[\text{C}_{10}\text{O}_8\text{H}_2] \cdot 4.8–5\text{H}_2\text{O}$ . It was analyzed from a tiny single crystal using a synchrotron microdiffraction setup installed at the ID13 station at ESRF (Grenoble, France). Its structure reveals a new mode of connection of aluminum-centered octahedra by edge-sharing, which is quite new in the crystal chemistry of extended MOF-type networks, involving aluminum. MIL-120 was further characterized by solid state NMR including <sup>27</sup>Al and <sup>13</sup>C nuclei. Porosity properties were examined from the adsorption of nitrogen and hydrogen at 77 K as well as at 303 K with carbon dioxide and methane. A thermal hydrogen desorption experiment was also analyzed. Adsorption energies for all these gases were measured directly via microcalorimetry and complete the examination of the porosity.

### Experimental Section

**Synthesis and Initial Characterization.** The aluminum pyromellitate (MIL-120) has been hydrothermally synthesized from a mixture of aluminum nitrate ( $\text{Al}(\text{NO}_3)_3 \cdot 9\text{H}_2\text{O}$ , Carlo Erba, 99+%), pyromellitic acid (1,2,4,5-benzenetetracarboxylic acid, noted H<sub>4</sub>btec,  $\text{C}_6\text{H}_2(\text{CO}_2\text{H})_4$ , Aldrich, 96%), sodium hydroxide

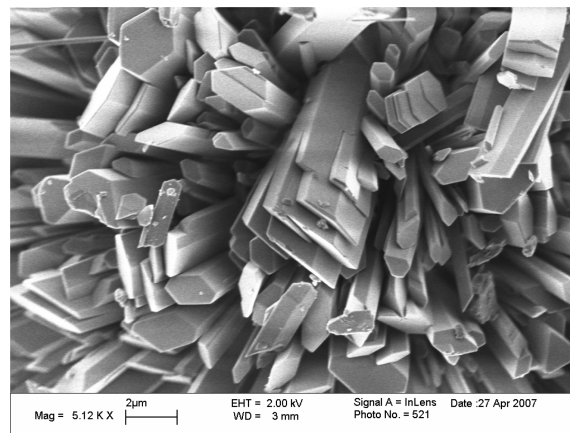


**Figure 1.** SEM image of the aluminum pyromellitate MIL-120 showing the platelike crystals with prismatic section.

solution (NaOH, 4M), and deionized water. A typical starting composition was 3.2 g of  $\text{Al}(\text{NO}_3)_3 \cdot 9\text{H}_2\text{O}$  (8.5 mmol), 0.5 g of H<sub>4</sub>btec (2 mmol), 3.4 mL of NaOH 4 M (13.6 mmol), and 20 mL of H<sub>2</sub>O (1111 mmol), and then, the resulting mixture was placed in a 125 mL Parr-type autoclave at 210 °C for 24 h. The pH was 12.2 before the hydrothermal treatment and then 1.85 at the end of the reaction. In comparison, the other aluminum pyromellitate MIL-118<sup>14</sup> appeared in more acidic condition from starting pH 2 to ending pH 0.9. It resulted in a white powdered product ( $\approx 0.7$  g), which was filtered off, washed with deionized water under reflux at 100 °C (in 300 mL H<sub>2</sub>O) for 10 h, and dried at room temperature. The scanning electron microscopy (SEM) examination (LEO 1530) showed that the MIL-120 compound consists of tiny prismatic platelike crystallites of 1–10  $\mu\text{m}$  size (Figure 1).

Elementary analysis was consistent with the chemical formula: Al, 17.65%; C, 20.61%; H, 3.41%. The calculated chemical formula from  $\text{Al}_4(\text{OH})_8[\text{C}_{10}\text{O}_8\text{H}_2] \cdot 5\text{H}_2\text{O}$  was as follows: Al, 18.50%; C, 20.54%; H, 3.42%.

**Single Crystal XRD analysis.** Two colorless platelike crystals of MIL-120 ( $2 \times 3 \times 10 \mu\text{m}$  size) were selected and attached under an optical microscope by Araldite to a tapered glass capillary using a *Kleindiek* MM3A micromanipulator. Due to the small size of the crystals, no absorption correction was applied. Experiments were performed at the ESRF ID13 undulator beamline<sup>12</sup> using a microdiffraction setup. The beam was monochromated to  $\lambda = 0.9613 \text{ \AA}$  by a liquid N<sub>2</sub> cooled Si-111 double crystal and focused to about  $1 \times 1 \mu\text{m}$  size by a crossed mirror system. In such a setup, the flux density at the sample within an about  $1 \times 1 \mu\text{m}^2$  effective beam reaches up to  $3 \times 10^{10}$  photons/sec/ $\mu\text{m}^2$ . The microgoniometer consisted of an air bearing spindle and a *Kleindiek* MM3A micromanipulator carrying a Hampton Research magnetic base. An *Olympus* microscope looking upstream along the beam path on the focus position was used for sample alignment in the focal spot. The optical alignment precision was below 1  $\mu\text{m}$ . The crystal was rotating during data collection with an angular step of 1°. Diffraction patterns were recorded by a MAR 165 CCD detector with  $2\text{K} \times 2\text{K}$  pixels of  $78.94 \times 78.94 \mu\text{m}^2$  and 16 bit readout. The diffraction patterns were processed with the XDS<sup>20</sup> software. Two data sets of 1 s per frame exposure time were collected on two different crystals of the sample and merged together using an XSCALE program within the XDS package.

- (12) Volkringer, C.; Popov, D.; Loiseau, T.; Guillou, N.; Férey, G.; Haouas, M.; Taulelle, F.; Mellot-Draznieks, C.; Burghammer, M.; Riekel, C. *Nat. Mater.* **2007**, *6*, 760.
- (13) Volkringer, C.; Loiseau, T.; Guillou, N.; Férey, G.; Elkaïm, E. *Solid State Sci.* **2009**, *11*, 1507.
- (14) Volkringer, C.; Loiseau, T.; Guillou, N.; Férey, G.; Haouas, M.; Taulelle, F.; Audebrand, N.; Margiolaki, I.; Popov, D.; Burghammer, M.; Riekel, C. *Cryst. Growth Des.* **2009**, *9*, 2927.
- (15) Barthelet, K.; Riou, D.; Nogués, M.; Férey, G. *Inorg. Chem.* **2003**, *42*, 1739.
- (16) Loiseau, T.; Muguerra, H.; Haouas, M.; Taulelle, F.; Férey, G. *Solid State Sci.* **2005**, *7*, 603.
- (17) Lin, Z.-Z.; Jiang, F.-L.; Chen, L.; Yuan, D.-Q.; Zhou, Y.-F.; Hong, M.-C. *Eur. J. Inorg. Chem.* **2005**, *77*.
- (18) Lin, Z.-Z.; Jiang, F.-L.; Yuan, D.-Q.; Chen, L.; Zhou, Y.-F.; Hong, M.-C. *Eur. J. Inorg. Chem.* **2005**, 1927.
- (19) Tian, Z.; Song, T.; Fan, Y.; Shi, S.; Wang, L. *Inorg. Chim. Acta* **2007**, *360*, 3424.

- (20) Kabsch, W. XDS. In *International Tables for Crystallography, Volume F. Crystallography of Biological Macromolecules*; Rossmann, M. G., Arnold, E., Eds.; Springer and IUCr: 2001; Chapter 25.2.9.

**Table 1. Crystal Data and Structure Refinement for MIL-120**

identification code	MIL-120
empirical formula	C <sub>10</sub> H <sub>20</sub> Al <sub>4</sub> O <sub>21</sub>
formula weight	584.18
temperature	100(2) K
wavelength	0.96130 Å
crystal system, space group	monoclinic, C2/m
unit cell dimensions	$a = 9.7480(10) \text{ \AA}$ $b = 20.0480(10) \text{ \AA}$ , $\beta = 134.42(1)^\circ$ $c = 7.4890(10) \text{ \AA}$
volume	1045.31 (26) Å <sup>3</sup>
Z, calculated density	2, 1.856 g/cm <sup>3</sup>
absorption coefficient	0.329 mm <sup>-1</sup>
F (000)	580
crystal size	2 × 3 × 10 μm
theta range for data collection	2.75 to 31.11°
limiting indices	$-10 \leq h \leq 10$ , $-20 \leq k \leq 20$ , $-7 \leq l \leq 7$
reflections collected/unique	5288/581
R (int)	0.1933
R <sub>mgd</sub> -F <sup>a</sup>	0.101
R <sub>sym</sub> /R <sub>mgd</sub> -F <sup>a</sup>	0.138/0.108 (crystal 1)
R <sub>sym</sub> /R <sub>mgd</sub> -F <sup>a</sup>	0.231/0.192 (crystal 2)
completeness to theta = 31.11	81.8%
refinement method	full-matrix least-squares on F <sup>2</sup>
data/restraints/parameters	581/2/94
goodness-of-fit on F <sup>2</sup>	0.964
final R indices [I > 2σ(I)]	R1 = 0.0818, wR2 = 0.2184
R indices (all data)	R1 = 0.0947, wR2 = 0.2322 R1 <sub>free</sub> = 0.0994
largest diff. peak and hole	0.562 and -1.018 e Å <sup>-3</sup>

<sup>a</sup>From ref 24.

The structural model was found by a direct method with SHELXS-86<sup>21</sup> software and developed by successive difference Fourier syntheses using SHELXL-97<sup>22</sup> software within WinGX<sup>23</sup> complex. Positions of hydrogen atoms belonging to OH groups were localized on difference maps. Hydrogen atoms belonging to the benzene ring were found using geometric constraints. Crystallographic data and parameters are presented in Table 1.

**Thermogravimetric (TG) and Thermodiffraction Analyses.** The TG experiments were carried out on a TA Instruments type 2050 thermoanalyzer TA under oxygen gas flow with a heating rate of 1 °C min<sup>-1</sup>. Variable-temperature in situ X-ray powder patterns were collected under static air in a Siemens D5000 diffractometer ( $\theta$ - $\theta$  mode) using cobalt radiation equipped with an Anton Parr HTK16 high temperature device and M Braun linear position sensitive detector (PSD). Each powder pattern was recorded in the range 8–45° (2 $\theta$ ) (at intervals of 20 °C up to 560 °C) with a 2 s/step scan, corresponding to an approximate duration of 1 h. The temperature ramp between two patterns was 5 °C min<sup>-1</sup>.

**Solid State NMR.** The high-resolution solid state <sup>13</sup>C magic angle spinning (MAS) NMR spectra were measured at 50.33 MHz, on a TecMag Apollo 200 NMR spectrometer, capable of high power <sup>1</sup>H-decoupling. The spinning rate used for <sup>1</sup>H-<sup>13</sup>C cross-polarization and magic angle spinning experiments was 10 kHz at ambient temperature. The spectrum was a result of the accumulation of 5120 scans. The recycle delay used was 10 s, the

$\pi/2$  pulse was 6 μs, and the contact time was 4 ms. The spectrum was referenced to adamantane, which showed two peaks at 29.6 and 38.5 ppm. <sup>27</sup>Al and <sup>1</sup>H MAS NMR spectra were recorded on a Bruker AVANCE 500 spectrometer (Larmor frequencies:  $\nu^{27}\text{Al} = 130.3 \text{ MHz}$ ;  $\nu^1\text{H} = 500.1 \text{ MHz}$ ) using a 2.5 mm MAS probe (Bruker Biospin). <sup>27</sup>Al MAS NMR ( $I = 5/2$ ) spectra were recorded with excitation pulse duration of 0.3 μs. A 1 M aqueous solution of Al(NO<sub>3</sub>)<sub>3</sub> was used as reference for the chemical shift of <sup>27</sup>Al. The recycle delay was chosen as 0.1 s. The spectra were fitted with the program DM2004.<sup>25</sup> <sup>1</sup>H MAS studies were made with a  $\pi/4$  pulse length of 3.7 μs and a recycle delay of 4 s. The accumulation number is 80. Values of the isotropic chemical shifts of <sup>1</sup>H are given with respect to TMS.

**Surface Area Measurement.** The porosity of MIL-120 was estimated by a gas sorption isotherm experiment in liquid nitrogen using the Micromeritics ASAP2010 apparatus. Before sorption measurements, the sample was outgassed under primary vacuum (5 Pa) at 200 °C for 15 h.

**Hydrogen Adsorption.** Hydrogen sorption properties are determined by measuring the pressure–composition isotherms (PCI) at 77 and 298 K and up to 8 MPa. The PCI curves are recorded using a volumetric device (Sievert's<sup>26</sup> method) equipped with calibrated and thermalized volumes and pressure gauges. The sample is enclosed in a stainless steel sample holder closed with a metal seal. Before any sorption measurements, the sample is outgassed under secondary vacuum at 200 °C for 10 h. The sample holder is immersed in a liquid N<sub>2</sub> Dewar at 77 K or in a thermalized water bath maintained at 298 K, and high purity hydrogen (6N) is introduced step by step up to 8 MPa. The pressure variations due to both gas cooling and hydrogen adsorption are measured after reaching thermodynamic equilibrium, usually in the range of minutes. The real equation of state for hydrogen gas is used from the program GASPAC V3.32 (Cryodata, Inc.<sup>27</sup>). The PCI curves are measured twice (i.e., two full adsorption–desorption cycles) in order to check the hysteresis effect and the measurement repeatability. All capacities reported here refer to the sample dry mass (i.e., outgassed mass). Sample volume correction is derived from density measurement obtained with a helium AccuPyc 1330 Micromeritics pycnometer. The measured sample density is 1.83 (±0.01) g/cm<sup>3</sup>.

**Hydrogen Thermal Desorption.** Thermal desorption studies have been performed by recording the total gas pressure (MKS absolute transducer) during hydrogen desorption under dynamic secondary vacuum. The sample was first cooled in hydrogen atmosphere (900 mbar) to 21 K by the help of a liquid He cryostat. The remaining gas that was not adsorbed by the sample at 21 K was removed by pumping to the secondary vacuum (10<sup>-5</sup> mbar). The adsorbed gas was thermally desorbed by applying a constant heating rate up to 150 K. Four different heating rates have been used in order to check the repeatability and the reversibility of hydrogen sorption. The total sample mass was 1.2 g.

**Adsorption Microcalorimetry.** The differential enthalpies of adsorption were obtained directly using two different Tian–Calvet type microcalorimeters each adapted to work either at 77 K or in the range from 298 to 473 K. Each of these

- (21) Sheldrick, G. M. *Acta Crystallogr.* **1990**, *A46*, 467.  
 (22) Sheldrick, G. M. *Acta Crystallogr. A* **2008**, *64*, 112.  
 (23) Farrugia, L. J. *J. Appl. Crystallogr.* **1999**, *32*, 837.  
 (24) Diederichs, K.; Karplus, P. *Nat. Struct. Biol.* **1997**, *4*, 269–275.

- (25) Massiot, D.; Fayon, F.; Capron, M.; King, I.; Le Calve, S.; Alonso, B.; Durand, J. O.; Bujoli, B.; Gan, Z. H.; Hoatson, G. *Magn. Reson. Chem.* **2002**, *40*, 70.  
 (26) Sieverts, A. Z. *Phys. Chem.* **1907**, *60*, 129.  
 (27) Lemmon, E. W.; Peskin, A. P.; McLinden, M. O.; Friend, D. G. *NIST12 Thermodynamic and Transport Properties of Pure Fluids V. 5.0*; Physical and Chemical Properties Division, National Institute of Standards and Technology: Boulder, Colorado, 2000.

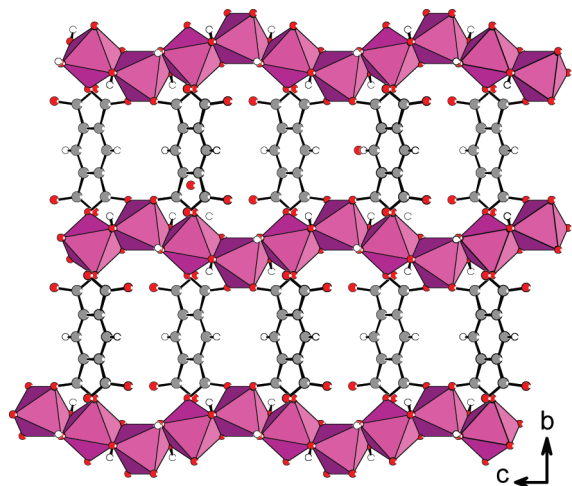


**Figure 2.** Representation of the structure of the aluminum pyromellitate  $\text{Al}_4(\text{OH})_8[\text{C}_{10}\text{O}_8\text{H}_2]$  (MIL-120) showing the infinite zigzag chains of edge-sharing aluminum octahedra running along the [102] direction with the  $-\text{trans-cis-trans-cis}-$  sequence. The chains are connected to each other through the pyromellitate linker.

devices are coupled to adapted gas dosing systems<sup>28</sup> built in house. At 77 K, the apparatus can measure adsorption enthalpies up to 1 bar; while at the higher temperature, the device is able to work up to 80 bar. For this latter experiment and in the present study, a temperature of 303 K was chosen and a final pressure of 20 bar was attained.

For these experiments, the sample (around 200 mg at 77 K and 700 mg at 303 K) is placed in the sample cell and, after outgassing to 200 °C for 16 h, the sample is placed into the appropriate microcalorimeter and attached to the gas dosing system.

For the experiment at 77 K, a quasi-equilibrium introduction of gas was used and, at 303 K, a stepwise introduction of gas was used. The errors in the enthalpy curves vary with the type of gas introduction but are on average around  $\pm 0.5 \text{ kJ mol}^{-1}$ .

## Results

**Structure Description.** The structure of the aluminum pyromellitate MIL-120 exhibits a novel three-dimensional open-framework built up from the connection of infinite inorganic chains with the btec ligand (Figure 2). There are two inequivalent crystallographic sites for aluminum residing on the special positions  $4g$  (2-fold axis for Al1) and  $4f$  (inversion center for Al2). Both aluminum cations are octahedrally coordinated with four oxygen atoms with typical Al–O distances ranging from 1.875(4) to 1.891(5) Å and attributed to bridging hydroxyl groups and two carboxyl oxygen atoms from the btec species, with slightly longer Al–O distances (1.931(5)–1.962(4) Å). Bond valence calculations<sup>29</sup> are in good agreement with the assignment of  $\mu_2\text{-OH}$  to the bridging oxygen atoms (1.08 and 1.09; expected value for OH: 1.2). However, the positions of  $\mu_2\text{-OH}$  and carboxyl oxygen differ in the two Al sites. For Al1, oxygen atoms from the carboxylate groups are located on two vertices of a common edge (equatorial position) in the octahedron and the remaining equatorial and apical vertices are

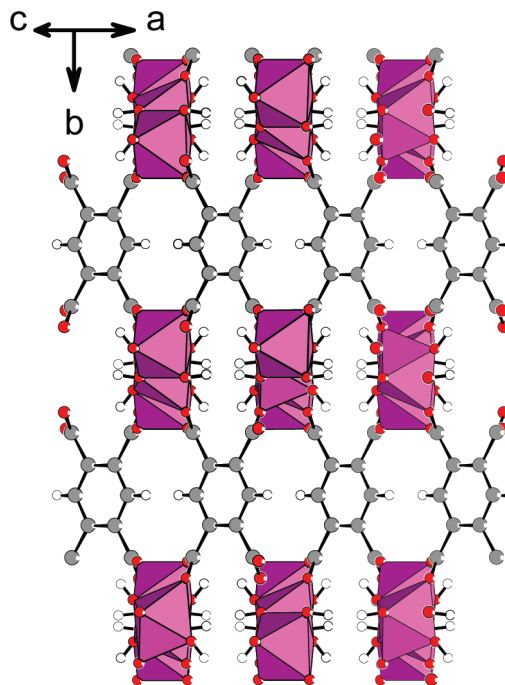


**Figure 3.** Connection mode of the pyromellitate ligand linking four distinct zigzag chains of aluminum-centered octahedra in MIL-120 along [102].

occupied by four  $\mu_2\text{-OH}$  groups. For Al2, the  $\mu_2\text{-OH}$  species are located on each vertex of the equatorial plane and the carboxyl oxygen atoms occupy the two apical positions of the octahedron. The aluminum cations are linked to each other with a strict alternation Al1–Al2 through the  $\mu_2\text{-OH}$  species by sharing a common edge. The two types of positions of the  $\mu_2\text{-OH}$  (equatorial and apical for Al1, equatorial for Al2) induce a  $\text{cis-trans}$  sequence of the connection mode, and this generates infinite chains running along the [102] direction (Figures 2 and 3). This type of configuration of chain is new in the crystal chemistry of MOF materials involving carboxylates with trivalent metals. Usually, the chains consist of the connection of  $\text{trans}$ -connected octahedral units generating straight rodlike inorganic building blocks (see for instance MIL-53,<sup>6</sup> MIL-69,<sup>8,9</sup> MIL-122,<sup>13</sup> and  $\text{Al}(\text{OH})(1,4\text{-ndc})\cdot 2\text{H}_2\text{O}$ <sup>10</sup>). The edge-sharing mode via  $\mu_2\text{-OH}$  is not so common for the aluminum carboxylates although it has been previously described in discrete molecular clusters, as for instance the binuclear (saccharate<sup>30</sup>), trinuclear (citrate<sup>31,32</sup>), and tetranuclear (malate<sup>33</sup>) units or the discrete octanuclear motif in the MOF solid MIL-110.<sup>12</sup> Four distinct zigzag inorganic wires are connected to each other along the [102] direction via the btec linker, which adopts a configuration  $\mu_8\text{-}\eta^1:\eta^1:\eta^1:\eta^1:\eta^1:\eta^1:\eta^1:\eta^1$ . Each carboxylate group is linked to two adjacent aluminum centers with a  $\text{syn-syn}$  bidentate bridging mode. It results in the formation of a

(28) Llewellyn, P. L.; Maurin, G. C. R. *Chimie* **2005**, *8*, 283.

(29) Brese, N. E.; O'Keeffe, M. *Acta Crystallogr., Sect. B* **1991**, *47*, 192.

(30) Lakatos, A.; Bertani, R.; Kiss, T.; Venzo, A.; Casarin, M.; Benetollo, F.; Ganis, P.; Favretto, D. *Chem.—Eur. J.* **2004**, *10*, 1281.

(31) Feng, T. L.; Gurian, P. L.; Healy, M. D.; Barron, A. R. *Inorg. Chem.* **1990**, *29*, 408.

(32) Malone, S. A.; Cooper, P.; Heath, S. L. *Dalton Trans.* **2003**, 4572.

(33) Happel, O.; Harms, K.; Seubert, A. *Z. Anorg. Allg. Chem.* **2007**, *633*, 1952.

three-dimensional network (Figure 4) with channels running along the  $c$  axis and delimited by the inorganic rodlike building block and the btec ligand, having their aromatic ring parallel to the  $c$  axis and perpendicular to the chains. The free diameter of the one-dimensional tunnels is  $5.4 \times 4.7$  Å. It was observed that water molecules reside within the channels, located on three distinct crystallographic sites with a ratio of  $5\text{H}_2\text{O}/4\text{Al}$ . Strong hydrogen bond interactions occurs between water molecules themselves ( $\text{OW1} \cdots \text{OW3} = 2.78(3)$  Å and  $\text{OW2} \cdots \text{OW3} = 2.65(3)$  Å) and between water molecules and hydroxo groups

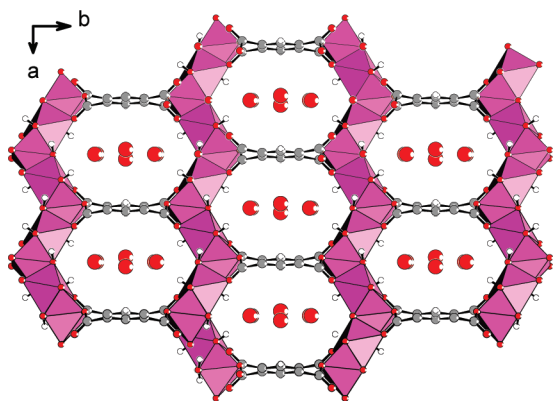


**Figure 4.** View of the structure of the aluminum pyromellitate  $\text{Al}_4(\text{OH})_8[\text{C}_{10}\text{O}_8\text{H}_2]$  (MIL-120) showing the tunnels running along the  $c$  axis.

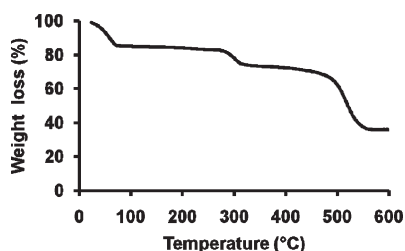


**Figure 5.** TG curve of the aluminum pyromellitate MIL-120 (under air, heating rate:  $1^\circ\text{C min}^{-1}$ ).

( $\text{OW1} \cdots \text{O1} = 2.82(1)$  Å and  $\text{OW2} \cdots \text{O2} = 3.05(1)$  Å) or carboxyl oxygen ( $\text{OW2} \cdots \text{O4} = 2.93(3)$  Å).

The thermogravimetric curve (Figure 5) of MIL-120 (Al) shows three weight loss events. The first step is assigned to the departure of trapped water molecules from room temperature to  $110\text{--}120^\circ\text{C}$ , with a weight value of 15% corresponding to  $4.8 \text{H}_2\text{O}$  per  $\text{Al}_4$  formula unit. The second weight loss (obs: 11.1%) occurs from 250 up to  $340^\circ\text{C}$ , and then, the last step corresponds to the value of 37.9% with a final plateau at  $560^\circ\text{C}$ . The total weight loss of the two last events (obs: 49.0%) is attributed to the departure of the organic linker ( $\text{H}_4\text{btec}$ ; calc: 43.8%) and  $2 \text{H}_2\text{O}$  (calc: 6.2%) coming from the dehydroxylation of the MIL-120 solid (total calculated weight loss: 50.0%). From this consideration, the second step could be assigned to the removal of  $2 \text{H}_2\text{O}$  together with  $\text{CO}_2$  coming from the partial decomposition of the pyromellitate molecule. The final weight loss up to  $560^\circ\text{C}$  is 36.0%, and this agrees with  $\text{Al}_2\text{O}_3$  (calc: 35.1%). The thermodiffractiongram (Supporting Information) indicates the increasing of the intensity of Bragg peaks upon encapsulated water removal from  $60^\circ\text{C}$  together with a slight shift toward high  $2\theta$  angles, reflecting a smaller cell volume for the empty pore structure. The diffraction peaks of MIL-120 are still visible up to  $340^\circ\text{C}$ , indicating that its structure is stable up to this temperature. Then, they disappear except those at the lowest angle  $9.5^\circ$  ( $2\theta$ ) and an additional peak around  $17.9^\circ$  ( $2\theta$ ). A difference of thermal stability is observed between the TG ( $280\text{--}300^\circ\text{C}$ ) and XRD ( $340^\circ\text{C}$ ) techniques and this may come from the inertia of the considered system since TG uses a small amount of sample ( $10\text{--}15 \text{mg}$ ) and XRD uses a large amount of sample ( $100\text{--}150 \text{mg}$ ) spread out on the surface of the platinum sample holder (4 cm length).

**Solid State NMR Characterization.** The 30 kHz-MAS  $^{27}\text{Al}$  NMR spectrum of MIL-120 (Figure 6) shows two partially resolved resonances with different quadrupolar parameters. Their isotropic chemical shifts (8.4 and 0.2 ppm) correspond to typical values of carboxylate-coordinated

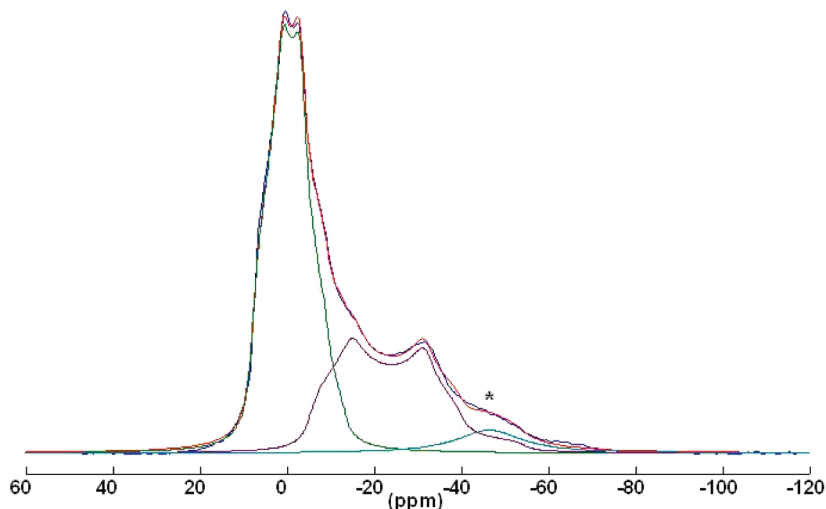


**Figure 6.**  $^{27}\text{Al}$  MAS NMR spectrum of the aluminum pyromellitate MIL-120 obtained with a 500 MHz spectrometer ( $\nu_{\text{rot}} = 30 \text{kHz}$  and number of accumulations of 4096), showing the different contributions: experimental spectrum (blue line); simulated spectrum (red line), and decomposition (green and purple lines). \* indicates impurity.

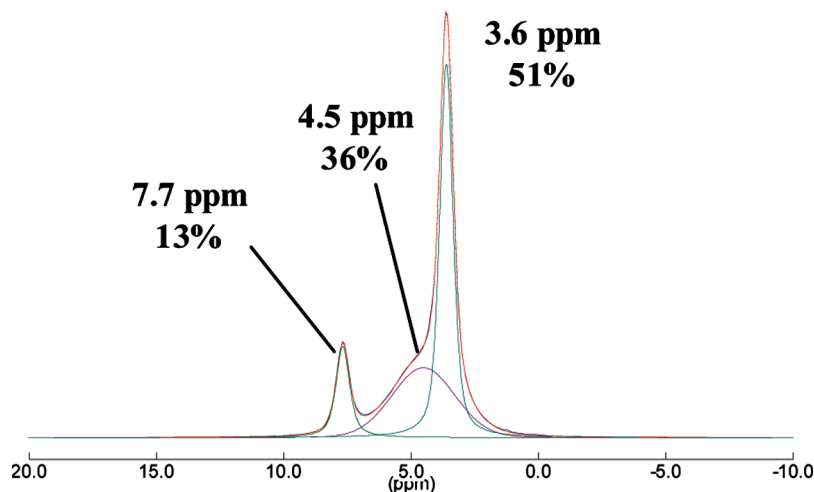


**Figure 7.**  $^1\text{H}$  MAS NMR spectrum of the aluminum pyromellitate MIL-120 obtained with a 500 MHz spectrometer ( $\nu_{\text{rot}} = 30$  kHz and number of accumulations of 80), showing the different contributions: experimental spectrum (blue line); simulated spectrum (red line), and decomposition (green and purple lines).

aluminum in an octahedral environment. For comparison, solution state NMR of aluminum citrate complexes showed signals within the broad range of 0 to 13 ppm.<sup>31,34</sup> Their signal area ratio of ca. 1 : 1 confirms the presence of two crystallographic Al sites within the structure of equal population, as determined previously by XRD analysis. The signal at 0.2 ppm exhibits a much larger quadrupolar coupling constant ( $C_Q = 8.07$  MHz) as a result of much distorted chemical environment around the corresponding Al compared to the second Al site with a  $C_Q = 4.77$  MHz. On the basis of these observations, assignment can be, therefore, provided. The Al1 site, where the carboxylate groups are connected through equatorial positions, should undergo more geometric distortion with respect to the more symmetric environment of Al2, where the carboxylate groups are bonded through axial positions. The signal at 0.2 ppm with  $C_Q = 8.07$  MHz should, therefore, correspond to Al1, while the one at 8.4 ppm with  $C_Q = 4.77$  MHz to Al2.

The solid state  $^1\text{H}$  NMR spectrum of MIL-120 (Figure 7) shows three signals at 3.6, 4.5, and 7.7 ppm. The signal at 3.6 ppm should correspond to protons of  $\mu_2$ -OH species linking the two Al. The broad signal around 4.5 ppm is characteristic of water molecules present within the pores and channels of the material. The signal at 7.7 ppm is attributed to the two aromatic protons present in btec moieties by comparison with the single signal at 8.0 ppm of  $\text{H}_4\text{btec}$  observed in a  $\text{DMSO-}d_6$  solution. Quantification allows one to determine the following molar ratio of  $\text{btec}/\text{H}_2\text{O}/\text{OH} \sim 1:3:8$  found in the materials, which agrees quite well with the corresponding values 1:5:8 from TGA and XRD analyses. The discrepancy in the water amount may arise from the NMR sample heating under high rotation frequency. Indeed, fast magic angle spinning can induce temperature increase inside the rotor to as

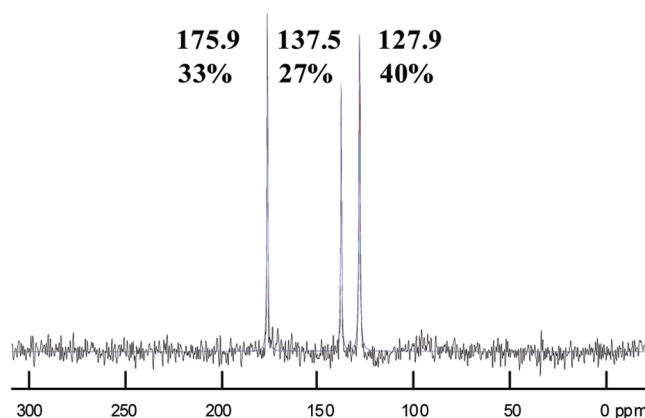


**Figure 8.**  $^{13}\text{C}\{^1\text{H}\}$  CPMAS NMR spectrum of the aluminum pyromellitate MIL-120 obtained with a 200 MHz spectrometer ( $\nu_{\text{rot}} = 10$  kHz and number of accumulations of 5120), showing the different contributions: experimental spectrum (black line); simulated spectrum (blue line), and decomposition (red lines).

much as ca. 30 °C at around 25–30 kHz.<sup>35</sup> According to the TGA curve, the loss of two water molecules (6% of total weight) occurs at ca. 50 °C, which is approximately the NMR sample temperature.

The MAS  $^{13}\text{C}$  NMR spectrum of MIL-120 was consistent with a unique crystallographic btec ligand sitting in a particular position (2d) with a highly symmetric environment. It showed three separate resonances, two in the high field region, and one in the carbonyl region (Figure 8). Peaks in the high field region could be assigned to the aromatic carbons, bound to the protons ( $\delta = 127.9$  ppm), and bound to the carboxylates ( $\delta = 137.5$  ppm). In the carbonyl region, only one signal ( $\delta = 175.9$  ppm) was observed for the fully bound terminal carboxylate carbonyls. In  $\text{DMSO-}d_6$  solution, the three signals of  $\text{H}_4\text{btec}$  were observed at 128.4, 134.6, and 167.3 ppm, respectively. The low-field shift of about 9 ppm of the carboxylate carbon signal due to bounding to aluminum is comparable to the 6 to 7 ppm low-field shifts observed in

(34) Matzapetakis, M.; Kourgiantakis, M.; Dakanali, M.; Raptopoulou, C. P.; Terzis, A.; Lakatos, A.; Kiss, T.; Banyai, I.; Iordanidis, L.; Mavromoustakos, T.; Salifoglou, A. *Inorg. Chem.* **2001**, *40*, 1734.

(35) Martin, R. W.; Zilm, K. W. *J. Magn. Reson.* **2004**, *168*, 202.

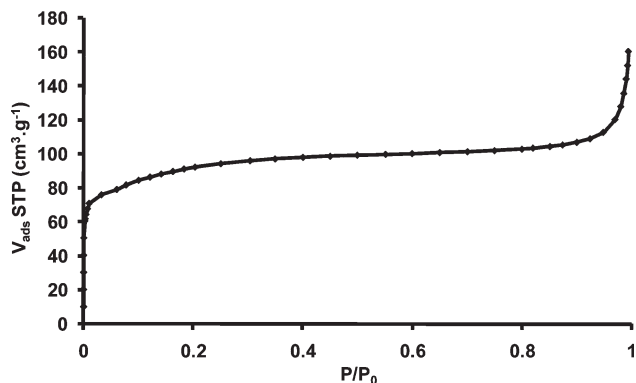


**Figure 9.** N<sub>2</sub> gas adsorption isotherm for the activated MIL-120 at 77 K.  $p/p_0$  is the ratio of gas pressure ( $p$ ) to saturation pressure ( $p_0$ ).

aluminum citrate complexes both in solid state and solution.<sup>34</sup> Recently, Loiseau et al.<sup>16</sup> reported the solid state <sup>13</sup>C spectrum of Ga(OH)(H<sub>2</sub>btec)·0.5H<sub>2</sub>O (MIL-61), which showed distinct signals for unbounded protonated carboxylic acid functions at 165.2 ppm and unprotonated gallium-bounded carboxylate functions at 175–176 ppm. Both situations are encountered in MIL-61, while in MIL-120 all carboxylate groups are deprotonated and bonded to aluminum.

**N<sub>2</sub> and H<sub>2</sub> Adsorption Properties.** The nitrogen sorption experiment (Figure 9) on the activated MIL-120 revealed a type I isotherm with a plateau at 100 cm<sup>3</sup> g<sup>-1</sup>, which is characteristic of a microporous solid. The measured Brunauer-Emmett-Teller (BET) surface area was estimated to be 308(4) m<sup>2</sup> g<sup>-1</sup> (within the range 0.06 <  $p/p_0$  < 0.2) with a micropore volume of 0.11 cm<sup>3</sup> g<sup>-1</sup>, and assuming a monolayer coverage by nitrogen, the Langmuir surface area was 432(1) m<sup>2</sup> g<sup>-1</sup>.

The adsorption microcalorimetry obtained with nitrogen at 77 K highlights this single adsorption step with a relatively constant energy of around -20 kJ mol<sup>-1</sup> (Figure 10). This behavior is reminiscent of that observed with zeolites in which micropore filling occurs although the value obtained here is larger than that observed with MFI-type zeolites<sup>36</sup> (for example, -14 to -17 kJ mol<sup>-1</sup>) which, thus, indicate relatively strong interactions with this gas. This may be due to the confined nature of the nitrogen in this porous structure.

The excess sorption isotherms of hydrogen measured at 77 and 298 K are shown in Figure 11. No adsorption/desorption hysteresis effects and good repeatability is noticed for all measurements. Both adsorption and desorption excess isotherms at 77 K show a type I behavior, which is typical for sorption on microporous solids.<sup>37</sup> At 298 K, the hydrogen uptake is linear with the applied pressure. This can be explained by Henry's law behavior for diluted layer adsorption on the surface. The excess hydrogen capacities at 3 MPa are 1.3 (±0.1) wt% and 0.2 wt% at 77 and 298 K, respectively. These values are in

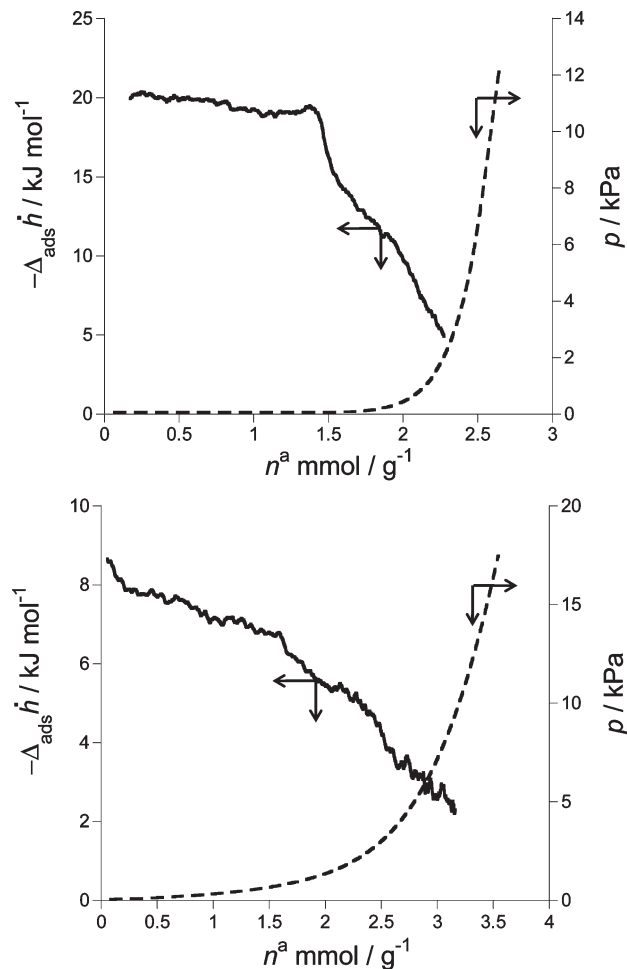


**Figure 10.** Differential enthalpies of adsorption and isotherm obtained at 77 K with nitrogen (top) and hydrogen (bottom) on MIL-120.

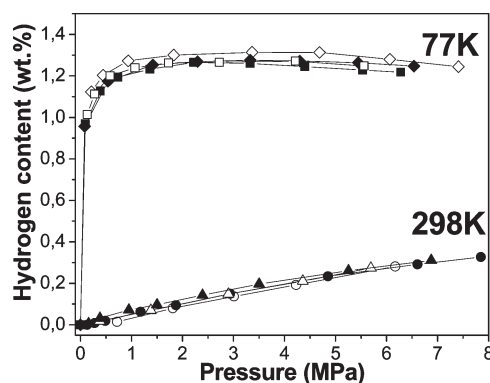


**Figure 11.** Pressure-Composition Isotherms of hydrogen in MIL-120 (Al) measured at 77 and 298 K. Full and open symbols represent adsorption and desorption, respectively.

good agreement with the general variation of hydrogen capacity as function of both specific surface area (BET) and microporous volume.<sup>38,39</sup> These studies have demonstrated a rough linear relationship between specific surface area and maximum excess hydrogen capacity at 77 K in different porous materials for specific surface area below 5000 m<sup>2</sup> g<sup>-1</sup>.

(36) Llewellyn, P. L.; Coulomb, J.-P.; Grillet, Y.; Patarin, J.; André, G.; Rouquerol, J. *Langmuir* **1993**, *9*, 1852.

(37) Sing, K. S. W.; Everett, D. H.; Haul, R. A. W.; Moscou, L.; Pierotti, R. A.; Rouquerol, J.; Siemieniowska, T. *Pure Appl. Chem.* **1985**, *57*, 603.

(38) Zhao, D.; Yuan, D.; Zhou, H.-C. *Energy Environ. Sci.* **2008**, *1*, 222.

(39) Thomas, K. M. *Catal. Today* **2007**, *120*, 389.

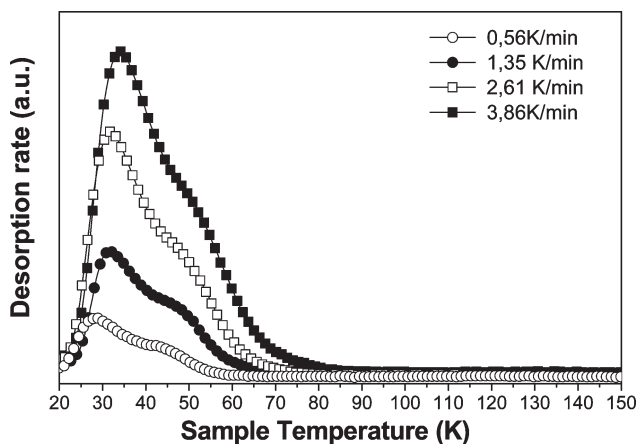


**Figure 12.** Hydrogen thermal desorption spectra of MIL-120(Al) for four heating rates 0.56 (○), 1.35 (●), 2.61 (□), and 3.86 K min<sup>-1</sup> (■).

The enthalpies of adsorption obtained for hydrogen adsorption at low coverage and at 77 K show an interaction of around  $-8 \text{ kJ mol}^{-1}$  (Figure 10). This value is typical of other microporous MOF materials such as MIL-91,<sup>40,41</sup> ScBDC,<sup>40,42,43</sup> and STA-12.<sup>44</sup> However, this value is slightly higher than the adsorption energies observed with MIL-47 and MIL-53<sup>45</sup> but lower than MOF's in which specific sites such as coordinatively active sites are present as the case for MIL-100(Cr).<sup>46</sup> This interaction varies gradually from  $-8$  to  $-5 \text{ kJ mol}^{-1}$  at around an uptake of  $2 \text{ mmol g}^{-1}$ , and after this, a stronger decrease is observed which would seem to mark the end of pore filling at this temperature.

**Hydrogen Thermal Desorption Properties.** The hydrogen thermal desorption results are displayed in Figure 12. Four different heating rates have been applied from 0.56, 1.35, and 2.61 to 3.86 K min<sup>-1</sup> showing good repeatability and complete reversibility of hydrogen sorption.

The gas desorption takes place between 22 and 80 K for all recorded spectra indicating a weak interaction between the gas molecules and MIL-120, as expected for gas physisorption. At higher temperature, the amount of desorbed gas is negligible.

All curves exhibit two desorption peaks: a first peak at low temperature and a second peak at temperature around 20 K higher than the first one. The maximum desorption rate corresponding to the peak maximum slightly varies with increasing the heating rate: from 28 to 33 K and from 39 to 46 K for the first and second peak,

- (40) Llewellyn, P. L. Universités Aix-Marseille I, II, III, Unpublished results, 2009.
- (41) Serre, C.; Groves, J. A.; Lightfoot, P.; Slawin, A. M. Z.; Wright, P. A.; Stock, N.; Bein, T.; Haouas, M.; Taulelle, F.; Férey, G. *Chem. Mater.* **2006**, *18*, 1451.
- (42) Miller, S. R.; Wright, P. A.; Serre, C.; Loiseau, T.; Marrot, J.; Férey, G. *Chem. Commun.* **2005**, 3850.
- (43) Perles, J.; Iglesias, M.; Martín-Luengo, M. A.; Monge, M. A.; Ruiz-Valero, C.; Snejko, N. *Chem. Mater.* **2005**, *17*, 5837.
- (44) Miller, S. R.; Pearce, G. M.; Wright, P. A.; Bonino, F.; Chavan, S.; Bordiga, S.; Margiolaki, I.; Guillou, N.; Férey, G.; Bourrelly, S.; Llewellyn, P. L. *J. Am. Chem. Soc.* **2008**, *130*, 15967.
- (45) Salles, F.; Kolokolov, D. I.; Jobic, H.; Maurin, G.; Llewellyn, P. L.; Devic, T.; Serre, C.; Férey, G. *Phys. Rev. C* **2009**, *113*, 7802.
- (46) Latroche, M.; Surlblé, S.; Serre, C.; Mellot-Draznieks, C.; Llewellyn, P. L.; Lee, J.-H.; Chang, J.-S.; Jhung, S. H.; Férey, G. *Angew. Chem., Int. Ed.* **2006**, *45*, 8227.

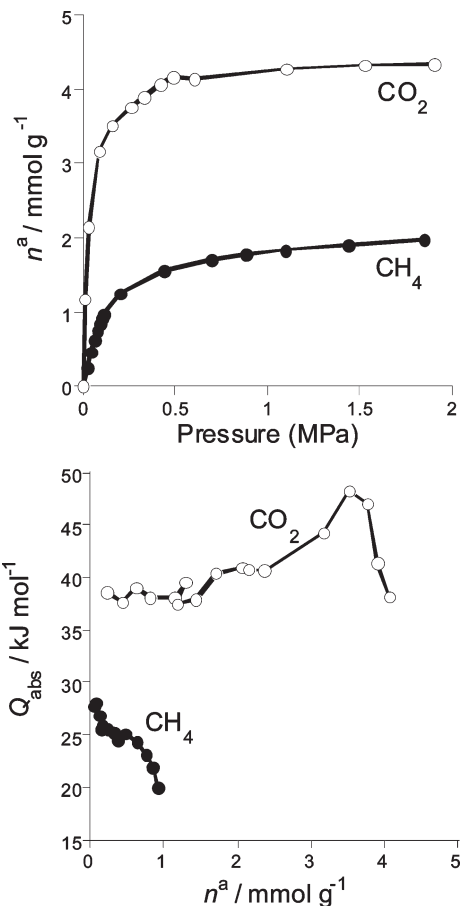


**Figure 13.** Isotherms (top) and differential enthalpies of adsorption (bottom) at 303 K obtained with carbon dioxide and methane on MIL-120.

respectively. Moreover, the intensity of the desorption peaks are directly proportional to the heating rates. These features are typical for the thermo-desorption technique. The presence of two distinct desorption peaks is attributed to the possible existence of two sorption sites with different enthalpies and geometries as previously reported in other compounds.<sup>47</sup>

**CO<sub>2</sub> and CH<sub>4</sub> Adsorption Properties.** The results obtained after the adsorption of methane and carbon dioxide at 303 K are shown in Figure 13. The isotherms show quite steep uptake at low pressure with a plateau in the uptake above a pressure of around 1 MPa in each case ( $4.2 \text{ mmol g}^{-1}$  for CO<sub>2</sub> and  $1.8 \text{ mmol g}^{-1}$  for CH<sub>4</sub>). This behavior, observed for both solids, reflect the microporous nature of the sample which is similar to the adsorption behavior of many zeolites including faujasites and MFI-type zeolites.<sup>48</sup> Indeed as an example, the uptakes observed for CO<sub>2</sub> with MIL-120 are between those measured for ZSM-5 (around  $3 \text{ mmol g}^{-1}$ )<sup>48,49</sup> and NaX ( $7$  to  $8 \text{ mmol g}^{-1}$ ).<sup>48,50</sup>

- (47) Panella, B.; Hönes, K.; Müller, U.; Trukham, B.; Schibert, M.; Pünter, H.; Hirscher, M. *Angew. Chem., Int. Ed.* **2008**, *47*, 2138.
- (48) Bourrelly, S.; Maurin, G.; Llewellyn, P. L. *Stud. Surf. Sci. Catal.* **2005**, *158*, 1121.
- (49) Dunne, J. A.; Mariwala, R.; Rao, M.; Sircar, S.; Gorte, R. J.; Myers, A. L. *Langmuir* **1996**, *12*, 5888.
- (50) Dunne, J. A.; Rao, M.; Sircar, S.; Gorte, R. J.; Myers, A. L. *Langmuir* **1996**, *12*, 5896.

Turning to the enthalpies of adsorption measured with MIL-120, both methane and carbon dioxide show quite high values with respect to many other MOF systems. This is especially the case for methane in which the  $-27 \text{ kJ mol}^{-1}$  obtained with MIL-120 can be compared with initial enthalpies between  $-15$  and  $-17 \text{ kJ mol}^{-1}$  for the MIL-47(V) and related MIL-53(Cr) and MIL-53(Al) systems.<sup>51</sup> Even for MOF's with coordinatively active sites (cus) such as MIL-100(Cr) or MIL-101(Cr), the initial enthalpies obtained with methane are only around  $-19 \text{ kJ mol}^{-1}$ .<sup>52</sup> This result, thus, highlights the effect of confinement of the probe molecule on adsorption.

This confinement effect can further be appreciated for the adsorption of carbon dioxide. In this study, values of around  $-37$  to  $-38 \text{ kJ mol}^{-1}$  are measured which are well above those of  $-20$  to  $-24 \text{ kJ mol}^{-1}$  measured for the MIL-47(V) and related MIL-53(Cr) and MIL-53(Al) systems.<sup>51</sup> On the other hand, where specific adsorption sites are present for  $\text{CO}_2$ , such as the cus mentioned above, higher adsorption energies are observed. This is the case for MIL-100(Cr) ( $-62 \text{ kJ mol}^{-1}$ ) and MIL-101(Cr) ( $-45 \text{ kJ mol}^{-1}$ ).<sup>52</sup> While the enthalpies observed with methane decrease with increasing coverage, those observed with carbon dioxide show a slight increase. This behavior is in contrast with that observed with other MOF materials but resemble that of zeolites and in particular the pure silica faujasite, DAY.<sup>53</sup> In the case of DAY, this increase in enthalpies is explained by a homogeneous (constant) interaction of the  $\text{CO}_2$  with the pore surface and a  $\text{CO}_2$ - $\text{CO}_2$  lateral interaction, which increases with increasing concentration in the pore. In the present case, a similar explanation can be retained and it is further of interest to note that, in the case of DAY, an initial interaction of  $-17 \text{ kJ mol}^{-1}$  was observed which is much lower than in the present case. These results, thus, suggest that the MIL-120 surface is quite homogeneous

from an energetic standpoint and that the relatively small pore size plays a distinct role with respect to enhanced confinement effects with the probe molecules studied.

## Conclusion

In this study, we described the hydrothermal synthesis and the structure of a MOF-type aluminum pyromellitate (MIL-120), which exhibits a new type of open framework. In this structure, the aluminum cations are linked to each other via a common edge of  $\mu_2$ -hydroxo groups, with a cis-trans sequence, in order to form infinite chains. This configuration is quite new for 3D networks involving trivalent metals since trans-connected corner-sharing octahedra were most commonly observed in other members of the MOF-type series. Moreover, with other complexing agents like phosphate, the occurrence of such chains of edge-sharing aluminum-centered octahedra was not reported although it was encountered in some other parent *p* elements like gallium in the organically templated phosphates MIL-35<sup>54</sup> or JGP-5.<sup>55</sup> This example illustrates the variety of connection modes of octahedrally coordinated trivalent metals in the presence of carboxylates for making infinite extended networks. The MIL-120 framework exhibits porosity properties with a BET surface area of  $308(4) \text{ m}^2 \text{ g}^{-1}$ . It is able to adsorb some gases such as hydrogen (at 77 K under 3 MPa), methane, or carbon dioxide ( $1.8 \text{ mmol g}^{-1}$  and  $4.2 \text{ mmol g}^{-1}$ , respectively, at 303 K under 1 MPa).

**Acknowledgment.** The authors would like to thank Dr. Eric Leroy (ICMPE, Thiais, France) for his assistance with the SEM images and the French ANR project "MATHYSSE" for financial support.

**Supporting Information Available:** Atomic coordinates and X-rays thermodiffraction diagrams as well as cif file of MIL-120 (Al) (CIF and PDF). This material is available free of charge via the Internet at <http://pubs.acs.org>.

- (51) Bourrelly, S.; Llewellyn, P. L.; Serre, C.; Millange, F.; Loiseau, T.; Férey, G. *J. Am. Chem. Soc.* **2005**, *127*, 13519.  
(52) Llewellyn, P. L.; Bourrelly, S.; Serre, C.; Vimont, A.; Daturi, M.; Hamon, L.; De Weireld, G.; Chang, J.-S.; Hong, D.-Y.; Hwang, Y.-K.; Jung, S. H.; Férey, G. *Langmuir* **2008**, *24*, 7245.  
(53) Maurin, G.; Llewellyn, P. L.; Bell, R. G. *J. Phys. Chem. B* **2005**, *109*, 16084.

- (54) Sassoey, C.; Loiseau, T.; Férey, G. *J. Fluorine Chem.* **2001**, *107*, 187.  
(55) Yang, Y.; Liu, Y.; Chen, C.; Wang, W.; Yi, Z.; W., P. *Polyhedron* **2004**, *23*, 1535.